Probing reaction dynamics in ^{12,13}C+^{119}Sn collisions

L.R. Gasques[1,*], *L.M.* Martinis[1], *L.C.* Chamon[1], *V.* Scarduelli[1], *W.A.Y.* Hatano[1], *J.K.L.* Chaves[1], *G.P.* Cessel[1], *M.A.G.* Alvarez[2], *J.P.* Fernández-García[2], and *L.* Garrido-Gómez[2]

[1]Universidade de Sao Paulo, Instituto de Fisica, Rua do Matao, 1371, 05508-090, Sao Paulo, SP, Brazil.
[2]Departamento FAMN, Universidad de Sevilla, Apartado 1065, 41080 Sevilla, Spain

Abstract. Elastic scattering of ^{12}C and ^{13}C projectiles on a ^{119}Sn target was investigated at $E_{\rm Lab}$ = 46.9 MeV, corresponding to energies slightly above the Coulomb barrier. The measurements were performed at the Open Laboratory of Nuclear Physics and Applications (LAFNA), University of São Paulo, using the STAR silicon detection array. Angular distributions were analyzed within the optical model and coupled-reaction-channels frameworks, adopting the São Paulo potential as the real bare interaction. For both systems, the inclusion of inelastic and one-nucleon transfer couplings in the coupled-reaction-channels calculations provided a consistent description of the data. Comparison between the ^{12}C and ^{13}C systems revealed clear isotopic effects, indicating that the valence neutron in ^{13}C enhances absorption from the elastic channel into non-elastic processes. These results contribute to a deeper understanding of coupling effects and nuclear structure influences in near-barrier heavy-ion reactions.

1 Introduction

Reactions induced by heavy ions at energies close to the Coulomb barrier provide a powerful means of investigating the interplay between nuclear structure and reaction dynamics. In this energy domain, elastic and inelastic scattering, transfer, and fusion processes are strongly affected by couplings to collective and single-particle excitations of the interacting nuclei. These effects, which go beyond the single-channel approximation, can be consistently described within the coupled-reaction-channels (CRC) framework [1, 2].

At the Open Laboratory of Nuclear Physics and Applications (LAFNA) of the Institute of Physics, University of São Paulo, a long-term experimental program has been devoted to the study of light- and medium-mass systems at near-barrier energies. Previous measurements have focused on reactions induced by weakly bound and cluster-type projectiles such as ^{6,7}Li and ^{10,11}B, allowing a detailed investigation of how binding energy and internal structure influence reaction mechanisms.

Within this context, reactions involving carbon isotopes have recently been explored. The ^{12}C nucleus, with its well-known three–α cluster configuration, plays a central role in both nuclear structure studies and stellar nucleosynthesis. Measurements for the ^{12}C+^{119}Sn system revealed a strong sensitivity of the angular distributions to couplings involving inelastic excitations and neutron transfer channels [3].

An analogous experimental investigation was performed for the ^{13}C+^{119}Sn system [4]. The addition of a valence neutron to the ^{12}C core introduces new coupling schemes, including one-neutron transfer, making this system particularly suitable for examining the impact of a moderately bound nucleon (S_n = 4.95 MeV) on near-barrier reaction dynamics.

Angular distributions for elastic scattering and reaction channels were measured for both systems at $E_{\rm Lab}$ = 46.9 MeV, approximately 10% above the Coulomb barrier. The analysis was carried out using the optical model and CRC formalisms, with the parameter-free São Paulo potential (SPP) [5] adopted as the bare interaction. The comparison between the two systems provides valuable insight into the influence of the valence neutron and the coupling effects that govern heavy-ion reactions near the Coulomb barrier.

2 Experimental setup

The experiments with ^{12}C and ^{13}C projectiles incident on ^{119}Sn targets were performed at the 30B beamline of LAFNA, Institute of Physics, University of São Paulo. In both cases, the beams were accelerated by the 8 MV tandem accelerator and directed onto self-supporting ^{119}Sn targets with areal densities of approximately 130 μg/cm^2. For normalization purposes, a thin ^{197}Au layer (~40 μg/cm^2) was evaporated onto the front surface of each target. At the energies and angles of the present experiment, the elastic scattering cross section on the gold layer is purely Rutherford and therefore provides an absolute normalization of the experimental cross sections. The average energy loss of the carbon ions at mid-target, about 100 keV, was taken into account in the analysis.

*e-mail: lgasques@if.usp.brauthor

© The Authors, published by EDP Sciences. This is an open access article distributed under the terms of the Creative Commons Attribution License 4.0 (https://creativecommons.org/licenses/by/4.0/).

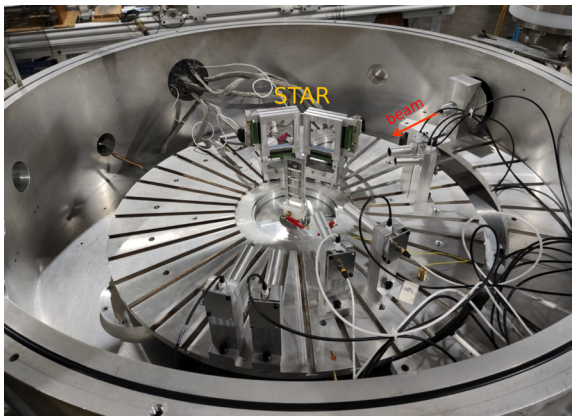

Figure 1. Internal view of the scattering chamber at the 30B beamline of LAFNA.

Charged reaction products were detected using the STAR (Silicon Telescopes Array for Reactions) detection system, positioned inside the 30B scattering chamber. The array consists of large-area segmented silicon detectors (50 mm × 50 mm) arranged in a triple-telescope configuration, providing both angular and energy resolution for light- and medium-mass ejectiles. The first detection stage is a thin single-sided silicon strip detector (SSSSD) with a nominal thickness of 20 μm, segmented vertically into 16 strips. The second stage, segmented horizontally, has a thickness between 300 and 400 μm. Together, these two stages form 256 (ΔE–E) pseudo-telescopes. A third, thick (1 mm) silicon pad detector placed behind the SSSSDs was used to stop high-energy light ions. A picture of the detection system setup is shown in Fig. 1. For the present measurements, the typical energy resolution of the STAR array was about 200 keV (FWHM).

3 Elastic Scattering Results

The present contribution focuses on the elastic scattering angular distributions for both systems. Detailed discussions of the inelastic, transfer, and other reaction channels can be found in Refs. [3, 4], where the complete CRC analyses are presented.

The inelastic couplings included in the CRC model are summarized in Table 1, which lists the spin, transition multipolarity, excitation energy, Coulomb transition probability, and deformation length for both projectile and target excited states. To determine the nuclear deformation parameters δ_λ from the Coulomb transition strengths, corrections due to the finite diffuseness of the nuclear density profile were taken into account [6, 7].

Table 2 presents the particle-core spectroscopic factors ($C^2S_{\ell j}$) values for all projectile and target overlaps included in the CRC scheme [3, 4]. A WS potential was assumed for the corresponding particle-core potentials. The respective parameters are listed in Table 3.

Elastic scattering angular distributions for the ^{12}C+^{119}Sn and ^{13}C+^{119}Sn systems were measured at $E_{\rm lab}$ = 46.9 MeV. The corresponding cross sections, normalized to the Rutherford values, are shown in Fig. 2,

Table 1. Spin, excitation energy (E^*, in MeV), transition multipolarity λ, transition strength from the ground-state (g.s.) to the excited states $B(E\lambda)\uparrow$ (in 10^{-3} e^{2}b$^\lambda$), and deformation length δ_λ (in fm) for the inelastic states included in the CRC calculations.

Nucl.	Spin	E^*	λ	$B(E\lambda)\uparrow$	δ_λ	Ref.
^{12}C	2^+	4.44	2	3.97	1.42	[8]
^{12}C	3^-	9.64	3	0.251	1.66	[9]
^{13}C	$\frac{1}{2}^+$	3.09	1	0.14	0.083	[10]
^{13}C	$\frac{3}{2}^-$	3.68	2	1.37	1.66	[11]
^{13}C	$\frac{5}{2}^+$	3.85	3	0.22	1.42	[11]
^{13}C	$\frac{5}{2}^-$	7.55	2	2.05	1.42	[11]
^{119}Sn	$\frac{3}{2}^+$	0.0239	2	4.87	0.14	[12]
^{119}Sn	$\frac{3}{2}^+$	0.920	2	125.	0.70	[3]
^{119}Sn	$\frac{5}{2}^+$	0.921	2	83.4	0.57	[3]
^{119}Sn	$\frac{5}{2}^+$	1.09	2	42.8	0.41	[3]
^{119}Sn	$\frac{5}{2}^+$	1.36	2	27.1	0.32	[3]
^{119}Sn	$\frac{5}{2}^+$	2.30	2	365	1.19	[3]

Table 2. Particle-core spectroscopic factors, $C^2S_{\ell j}$, for all projectile and target overlaps included in the CRC scheme. The parameter values of the WS potentials assumed for the cluster-core systems are also presented in the table.

Overlap	E^* (MeV)	State ($n\ell j$)	$C^2S_{\ell j}$
$\langle\, ^{13}$C $\mid\, ^{12}$C+n $\rangle$	0.0	$1p_{1/2}$	0.56
$\langle\, ^{119}$Sn $\mid\, ^{118}$Sn+n $\rangle$	0.0	$3s_{1/2}$	0.56
$\langle\, ^{12}$C $\mid\, ^{11}$B+p $\rangle$	0.0	$1p_{3/2}$	1.0
$\langle\, ^{120}$Sb $\mid\, ^{119}$Sn+p $\rangle$	0.0	$2d_{3/2}$	1.0
$\langle\, ^{120}$Sb $\mid\, ^{119}$Sn+p $\rangle$	0.5	$1g_{7/2}$	25
$\langle\, ^{120}$Sn $\mid\, ^{119}$Sn+n $\rangle$	0.0	$3s_{1/2}$	1.4
$\langle\, ^{120}$Sn $\mid\, ^{119}$Sn+n $\rangle$	2.8	$1h_{11/2}$	3.6
$\langle\, ^{14}$C $\mid\, ^{13}$C+n $\rangle$	0.0	$1p_{1/2}$	1.6
$\langle\, ^{119}$Sn $\mid\, ^{118}$Sn+n $\rangle$	0.0	$3s_{1/2}$	0.42

with the upper and lower panels referring to the ^{12}C and ^{13}C projectiles, respectively. It is worth mentioning that the yields corresponding to the $3/2^+$ excited state of ^{119}Sn at 23 keV could not be experimentally separated from those of the elastic channel. However, CRC calculations indicate that the contribution from this inelastic transition is negligible compared to the elastic scattering cross section and does not significantly affect the extracted data. In addition, the probability of exciting the 89 keV $11/2^-$ state in ^{119}Sn is expected to be very small, as it corresponds to a highly hindered magnetic hexadecapole (M4) transition involving a large angular momentum transfer (ΔL=4) and a change in parity.

Table 3. Parameter values of the WS potentials assumed for the cluster-core systems in the CRC transfer calculations. The V_0^{adj} values presented in the table provide the right results for the binding energy when the compound system is in its ground-state.

Composite system	V_0 (MeV)	R_0 (fm)	a (fm)
n+^{12}C	53.5	2.35	0.64
n+^{13}C	55.5	2.50	0.80
n+^{118}Sn	47.1	5.70	0.66
p+^{11}B	78.1	2.30	0.62
p+^{119}Sn	47.1	5.75	0.66
n+^{119}Sn	54.3	5.70	0.89

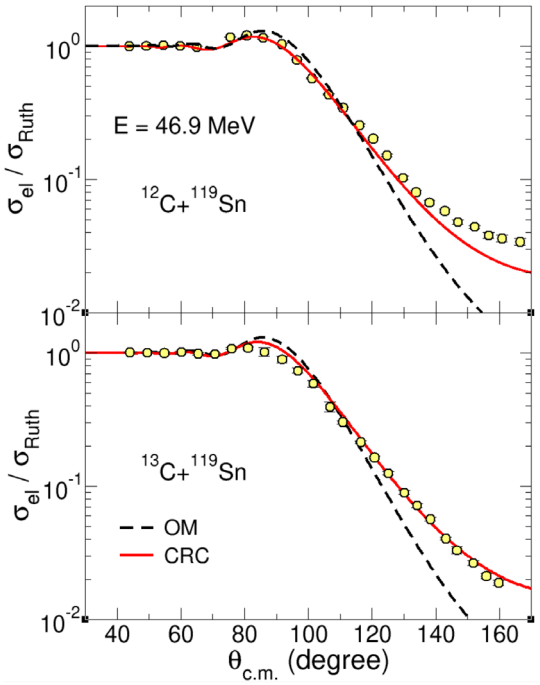

Figure 2. Elastic scattering angular distributions for (top) ^{12}C+^{119}Sn and (bottom) ^{13}C+^{119}Sn at $E_{\rm Lab}$ = 46.9 MeV. Experimental data (symbols) are compared with optical model (dashed lines) and CRC (solid lines) calculations using the SPP.

For both systems, calculations were performed using the SPP for the real part of the nuclear interaction. The imaginary part of the optical potential was described by a phenomenological Woods-Saxon (WS) form, with parameters W_0 = 80 MeV, r_{i0} = 0.8 fm, and a_i = 0.30 fm. With this choice, the imaginary strength in the surface region remains small, accounting only for flux absorption due to barrier penetration. The dashed lines in the figure represent single-channel optical model (OM) calculations, while the solid curves correspond to CRC results including inelastic and single-nucleon transfer couplings.

For the ^{12}C+^{119}Sn system, the CRC calculations reproduce the overall trend of the experimental data and represent a clear improvement over the single-channel description, particularly around the Coulomb–nuclear interference region ($\theta_{\rm c.m.} \sim 90°$). The attenuation of the CRC cross section in this region reflects the influence of couplings to non-elastic channels. Some underestimation of the data remains at large scattering angles, possibly due to high-lying excited states not explicitly included in the model space [13–16]. A similar behavior is observed for the ^{13}C+^{119}Sn system, where the inclusion of couplings also improves the description of the data. Overall, the CRC framework provides a consistent and physically meaningful representation of the elastic scattering for both systems.

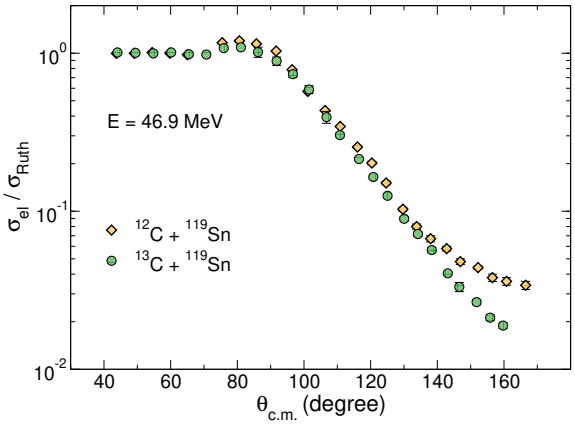

Figure 3. Experimental cross sections for the elastic scattering of ^{12}C+^{119}Sn and ^{13}C+^{119}Sn at $E_{\rm Lab}$ = 46.9 MeV.

Fig. 3 presents a direct comparison between the measured angular distributions for both systems. At larger scattering angles ($\theta_{\rm c.m.} > 130°$), Fig. 3 shows noticeable differences between the ^{12}C and ^{13}C elastic angular distributions. This observation indicates that, at this energy, the presence of an additional neutron in the projectile enhances the absorption of flux from the elastic channel into non-elastic processes.

4 Conclusions

Elastic scattering angular distributions for the ^{12}C+^{119}Sn and ^{13}C+^{119}Sn systems were measured at $E_{\rm Lab}$ = 46.9 MeV, corresponding to energies slightly above the Coulomb barrier. The experimental data were analyzed within the OM and CRC frameworks using the SPP as the bare interaction.

For both systems, the inclusion of inelastic and single-nucleon transfer couplings in the CRC calculations significantly improved the description of the measured cross sections, particularly in the Coulomb–nuclear interference region. The comparison between the two isotopic systems revealed clear differences in the angular distributions, most notably at large scattering angles. These differences are interpreted as arising from the additional coupling schemes introduced by the valence neutron in ^{13}C, which enhances the absorption of flux from the elastic channel into non-elastic processes.

The results confirm the sensitivity of near-barrier heavy-ion scattering to nuclear structure effects and demonstrate the capability of the CRC approach to provide a consistent description of such phenomena. Future work will include a systematic investigation of other carbon isotopes on tin and lead targets, aiming to further explore the role of weakly and moderately bound nucleons in heavy-ion reaction dynamics.

References

[1] D. Ridikas et al., Nucl. Phys. A **628**, 363 (1998), https://doi.org/10.1016/S0375-9474(98)00657-5

[2] N. Keeley, N. Alamanos, N. Single, Phys. Rep. 75, 054610 (2007), https://doi.org/10.1103/PhysRevC.75.054610

[3] L. M. Martinis, et al., Phys. Rev. C 111, 034615 (2025), https://doi.org/10.1103/PhysRevC.111.034615

[4] L. M. Martinis, et al., Eur. Phys. J. A. 62, 46 (2026), https://doi.org/10.1140/epja/s10050-026-01823-6

[5] L. C. Chamon, et al., Phys. Rev. C 66, 014610 (2002), https://doi.org/10.1103/PhysRevC.66.014610

[6] D.F.M. Botero, L.C. Chamon, B.V. Carlson, J. Phys. G 44, 105,102 (2017), https://doi.org/10.1088/1361-6471/aa846e

[7] L. C. Chamon, B.V. Carlson, Nucl. Phys. A 846, 1 (2010), https://doi.org/10.1016/j.nuclphysa.2010.06.003

[8] B. Pritychenko, M. Birch, B. Singh, M. Horoi, Atomic Data and Nucl. Data Tables 107, 1 (2016), https://doi.org/10.1016/j.adt.2015.10.001

[9] B. John, et al., Phys. Rev. C 68, 014305 (2003), https://doi.org/10.1103/PhysRevC.68.014305

[10] E. K. Warburton, D. E. Alburger, D. J. Millener, Phys. Rev. C 22, 2330 (1980), https://doi.org/10.1103/PhysRevC.22.2330

[11] S. A. Goncharov et al., Phys. Atom. Nuclei 85, 785 (2022), https://doi.org/10.1134/S1063778823010210

[12] D. M. Symochko, E. Browne, J. K. Tuli, Nucl. Data Sheets 110, 2945 (2009), https://doi.org/10.1016/j.nds.2009.10.003

[13] M. Evers, et al., Phys. Rev. C 78, 034614 (2008), https://doi.org/10.1103/PhysRevC.78.034614

[14] L. C. Chamon, et al., J. Phys. G 42, 055102 (2015), https://doi.org/10.1088/0954-3899/42/5/055102

[15] L. C. Chamon, L. R. Gasques, J. Phys. G 43, 015107 (2016), https://doi.org/10.1088/0954-3899/43/1/015107

[16] L. C. Chamon, L. R. Gasques, J. C. Zamora, J. Phys. G 47, 105103 (2020), https://doi.org/10.1088/1361-6471/aba424